Current Conduction Mechanisms in *n*-type *a*-SiGe:H/*p*-type *c*-Si Heterojunctions

P. Rosales-Quintero*, A. Torres-Jacome, F. J. De la Hidalga-Wade, C. Zúñiga-Islas,
W. Calleja-Arriaga, and C. Reyes-Betanzo
Departamento de Electrónica, Instituto Nacional de Astrofísica, Óptica y Electrónica (INAOE).
AP 51 & 216, C.P 72000, Puebla, Pue., México.
(Recibido: 20 de enero de 2007; Aceptado: 10 de marzo de 2008)

n-type *a*-SiGe:H/*p*-type *c*-Si heterojunctions, fabricated with two different base doping concentrations (7×10^{17} and 5×10^{18} cm^{-3}) and two thicknesses (37 and 200 nm) for the *n*-type *a*-SiGe:H film, were electrically characterized. The current transport mechanisms were determined by analyzing the temperature dependence of the current-voltage characteristics. The electrical measurements show that at low forward bias ($V < 0.45$ V) the transport mechanisms depend on both the base doping concentration and the thickness of the amorphous film. On the other hand, at higher forward bias ($V > 0.45$ V) the space-charge limited effect becomes the main transport mechanism for all the measured devices. The increase of both, base doping concentration and layer thickness, leads to an increase of the reverse leakage current. Using high-frequency capacitance-voltage characteristics both type of heterojunctions have shown an abrupt junction behavior. The Anderson rule was used to determine the conduction and valence band discontinuities for these heterojunctions.

Keywords: Amorphous semiconductors; Heterojunction diodes; Transport mechanisms; Leakage currents

1. Introduction

In recent years, the electronic and thermal properties of *a*-SiGe:H films have been improved by means of the Plasma-Enhanced Chemical Vapor Deposition (PECVD) technique using frequencies lower than the typical deposition frequency of 13.5 MHz [1,2]. These low-frequency PECVD films have been used for the fabrication of several optoelectronic and thermal devices such as solar cells, photodetectors, and bolometers [3-6]. Nevertheless, other applications for these amorphous films, e.g. Heterojunction Bipolar Transistors (HBT), require a better understanding of the physical properties and current transport mechanisms which determine their electrical behavior. Up to now the charge transport mechanisms in amorphous/crystalline heterojunctions are not fully understood. Several mechanisms have been proposed to explain the *J-V* characteristics of *a*-Si:H/crystalline heterojunctions: multi-tunneling capture-emission (MTCE) [7]; recombination at the space charge-region [8,9]; and thermionic emission (TE) [10,11]. Recently, it has been shown that the transport mechanisms are strongly dependent on the thickness of the amorphous film [12]. This reference also showed that the heterojunctions with a thin *n*-type *a*-SiGe:H emitter have an ideality factor ~1 and the valence band discontinuity is much higher than that in the conduction band. These parameters suggest that this type of amorphous films could be used as the base material for improving the electrical behavior of HBT devices.

Thus, the electrical characterization of *n*-type *a*-SiGe:H films used as the emitter in heterojunctions, for two different base doping concentrations and two thicknesses, is presented in this work. In Section II the fabrication steps are described. Section III presents the *C-V* and *J-V-T* characteristics, and the results are discussed. Finally, the conclusions of this work are presented in Section IV.

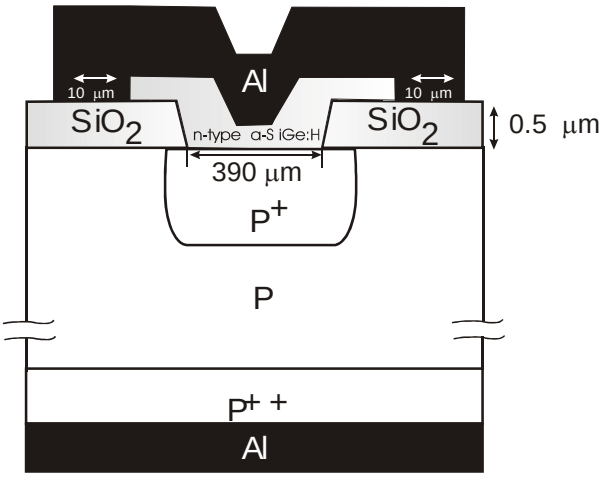

Figure 1. Cross-section of the n-type a-SiGe:H/ p-type c-silicon heterojunction. The area is 1.13×10^{5} $(\mu m)^{2}$.

2. Experimental

The cross section of the fabricated *n*-type *a*-SiGe:H/*p*-type *c*-Si heterojunctions is shown in Fig. 1. The substrates were boron doped silicon (100) wafers with an average concentration of 1×10^{15} cm^{-3}. First, boron diffusion was performed at the bottom of the wafer in order to obtain the back contact, and 500 nm of silicon oxide was grown thermally on the top surface. Windows were opened on the silicon oxide using photolithography; these windows define the area of the heterojunctions. Next, a boron implantation was performed on four wafers at 40 keV through a 120 nm oxide. Two different doses were used in order to obtain two different base doping concentrations (Table I). Next, the wafers were annealed for 15 min in steam followed by 90 min in nitrogen, at 1100 º C, with the purpose of reducing

* prosales@inaoep.mx

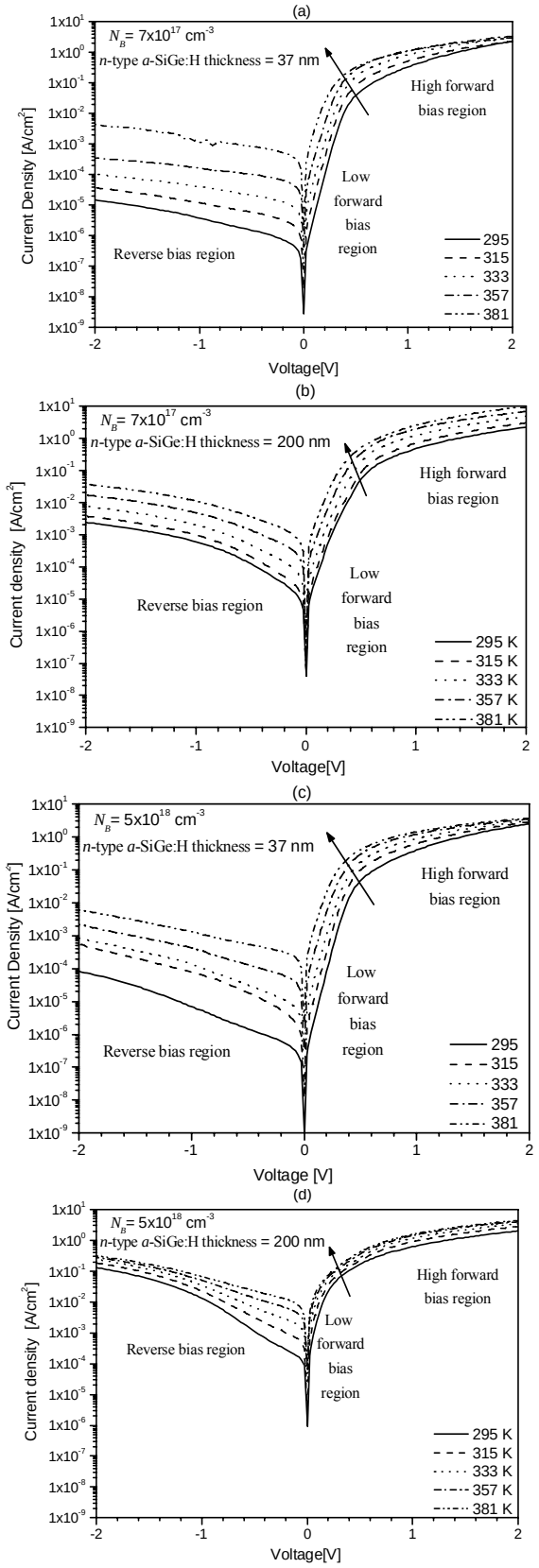

Figure 2. *J-V* characteristics of the *n*-type *a*-SiGe:H/ *p*-type *c*-silicon heterojunctions at different temperatures.

the implantation damage and to electrically activate the implanted impurities. Then, after performing the cleaning and hydrogen passivation steps of the substrates, *n*-type *a*-SiGe:H films (for 37 and 200 nm-thick) were deposited on the wafers (for both boron surface concentrations 7×10^{17} and 5×10^{18} cm^{-3}). Finally, aluminum was e-beam evaporated on both surfaces of the wafers. The *a*-SiGe:H films were deposited using a low-frequency (110 kHz) PECVD system at 300 °C. The precursor gases were SiH_4 and GeH_4 with hydrogen dilution. The gas flow ratio R = $[GeH_4]/[GeH4+SiH_4]$ was set to 1/10, and the *n*-type doping was achieved by adding phosphine to the reactive gases using a gas flow ratio of R = $[PH_3]/[SiH_4+GeH_4+PH_3]$ = 1/6. The measured optical band gap ($Eg_{\,n\text{-}type\ a\text{-}SiGe:H}$) was 1.4 eV corresponding to a germanium content of $X \approx 44\ \%$ according to $Eg = 1.76-0.78X$ [13].

3 Results and discussion

A. Current density - voltage characteristics

The *J-V* characteristics were measured using an HP4156B semiconductor parameter analyzer, for temperatures in the 295 - 381 K range, and the results are shown in Fig. 2. It can be seen that all the heterojunctions show two different operating regions at forward current density. For $V < 0.45$ V, the current density increases exponentially as a function of the applied voltage, and the *J-V* behavior can be described by [14]:

$$J = J_0\left[\exp[AV]-1\right] \tag{1}$$

where A is a coefficient defined by

$$A = \frac{q}{\eta\, kT} \tag{2}$$

Where η is the ideality factor, and J_0 is the saturation current density defined by:

$$J_0\ \alpha\ \ \exp\left[-\frac{E_{ac}}{kT}\right] \tag{3}$$

In eq. (3) E_{ac} is the activation energy measured with respect to the valence band, k is the Bolztmann's constant, and T is temperature in Kelvin. As can be seen from eqs. (2) and (3) the current density is a function of temperature, and the transport mechanisms can be identified analyzing the temperature dependence of A and J_0. For instance, if the forward-bias transport were limited by diffusion, A would show a linear behavior corresponding to η = 1 and E_{ac}=E_g. On the other hand, the transport would be limited by recombination at the depletion region if A showed a linear behavior and η =2 and E_{ac}=E_g/2. It is worth

Table 1. Dose and peak of the doping concentration on the wafers and thickness of the amorphous films

Wafer	Dose [cm^{-2}]	Peak concentration [cm^{-3}]	*n*-type *a*-SiGe:H thickness [nm]
W1	5×10^{13}	7×10^{17}	37
W2	5×10^{13}	7×10^{17}	200
W3	5×10^{14}	5×10^{18}	37
W4	5×10^{14}	5×10^{18}	200

mentioning that the exact value η = 2 can be obtained only when a single recombination level located at midgap is assumed. When a continuous trap distribution is assumed, the value of η is in the range 1-2. Finally, if the current density were controlled by tunneling**,** *A* would be independent of the temperature. It must be emphasized that different transport processes may be occurring at the barrier of the heterojunction, whereas the measured current density will usually be dominated by only one of the transport mechanisms [15]. A summary of the several charge transport mechanisms is given in Table II.

For all the diodes measured and forward voltages above 0.45 V, in all measured diodes, the *J-V* characteristics deviated from the ideal behavior. If the curves from Fig. 2 were plotted in a log-log scale for *V* > 0.45 V, the *J-V* characteristics would show a power law dependence; therefore, *J* presents a space charge limited characteristic (SCLC) at high forward bias. For a SCLC condition, the relationship between *J* and *V* is described as [16]:

$$J = KV^{M} \tag{4}$$

where *K* is a function of the film thickness and trap distribution, while *M* depends on the density of states in the amorphous layer.

The parameters *A*, *Jo*, *K*, *M* and the series resistance (*Rs*) were determined by fitting the *J-V* characteristics, as a function of temperature, using the following equation [17]:

$$V = \frac{1}{A}\ln\left(\frac{J}{J_0}+1\right) + \left\{\frac{J}{K + \dfrac{1}{Rs\left[V - \dfrac{1}{A}\ln\left(\dfrac{J}{J_0}+1\right)\right]^{M-1}}}\right\}^{1/M} \tag{5}$$

The Arrhenius plots of *A* and J_0 are shown in Fig. 3 for all the wafers. From Fig. 3(a), the value of η obtained was 1.28 for W1 and W3. Log (J_0) versus 1/*kT* shows a fairly linear behavior allowing for the determination of E_{ac} = 0.82 and 0.84 eV; this is shown in Fig. 3(b). As can be seen, the activation energy values are around 5*kT* eV from $E_{g\text{-}aSiGe:H}$ /2, and the ideality factor lies in the range 1-2. These results indicate that the recombination on the amorphous side of the space-charge region is the dominant mechanism. Regarding the W2 and W4 samples, we observe in Fig. 3(a) that *A* is almost independent of temperature showing that the dominant mechanism is tunneling [14]. Among the various tunneling mechanisms, the conduction seems to follow the multistep tunneling (MT) through the depletion region. This is reasonably explained by the increased probability of multistep tunneling due to the surface base doping concentration, the continuously distributed localized states within the band gap of the *a*-SiGe:H film, and the linear behavior of log (J_0) vs. *T* shown in Fig. 3(c). In the MT model, J_0 is described by [18]:

$$J_0 \alpha \exp[\gamma \beta T] \tag{6}$$

where γ depends weakly on temperature, and β is the proper temperature coefficient that describes the linear dependence on temperature of the mobility gap and the Fermi level position in the *n*–type and *p*–type layers. By using the calculated slope from Fig. 3(b) and the typical value of β = 3 meV/K [18], we calculated an average γ of 18.4 eV^{-1}, which is in agreement with that reported in [18].

A linear relationship for all the heterojunctions is observed for the *M-1* vs 1000/*T* plots (Fig. 4(a)), with *M* ranging from 2.5 to 3.5 for W1 and W3, whereas *M* ranged from 3.2 to 3.8 for W2 and W4. These results agree with Rose's model, which was obtained assuming an exponential trap distribution [16]:

$$N_{TC}(E) = N_{TC0}\exp\left[\frac{E - E_C}{kT_0}\right] \tag{7}$$

where N_{TC0} is the density of states at the conduction band-edge tail, E_C is the conduction band edge, and T_0 is a temperature parameter that characterizes the trap distribution, which is calculated using the slope of the *M-1* vs. 1000/*T* curve. From Fig. 4 (a) we obtained $T_{0\ average}$ = 1440 and 564 K, corresponding to kT_0 = 124 and 48 meV for the *n*-type *a*-SiGe:H films with thicknesses of 37 and 200 nm, respectively. These kT_0 values show that the total density of states (DOS) in *n*-type *a*-SiGe:H is strongly dependent on its thickness. Our results suggest that the band tails broaden as the amorphous thickness is reduced [12]. Therefore, when the thickness of the *n*-type *a*-SiGe:H is 37 nm, the deep levels are covered by the tail states; whereas if the thickness of the n-type a-SiGe:H is 200 nm, the tail states do not cover the deep levels [12].

Based on these results, we can suggest that both, the base doping concentration and the contribution of localized

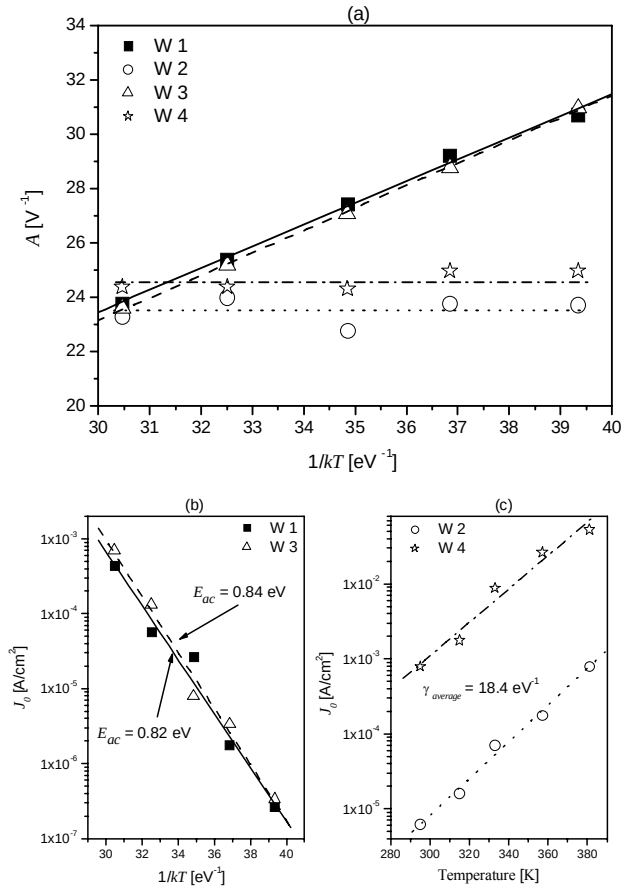

Figure 3. (a) Arrhenius plots of *A*. The values of η are 1.27 and 1.28 for W1 and W3, respectively. (b) Arrhenius plots of J_0. The calculated activation energies are 0.82 and 0.84 eV for W1 and W3, respectively. (c) J_0 as a function of temperature for W2, and W4. An average value of γ =18.4 eV^{-1} was calculated.

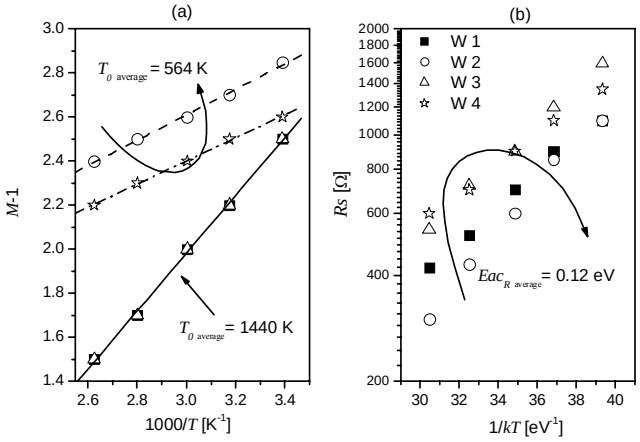

Figure 4. Dependence of *M-1* and *Rs* on temperature (SCLC region).

states distributed continuously in the band gap of the *n*-type *a*-SiGe:H, determine the dominant transport mechanism.

Thus, when the thickness of the *n*-type *a*-SiGe:H is 37 nm,
there is an increase of carriers recombination near the band edges through the tail states, which lowers η from 2 to 1. On the other hand, if the thickness of the *n*-type a-SiGe:H is 200 nm, the tail states do not cover the deep levels, therefore the midgap recombination increases. We can deduce that η is around 2, as we already reported in [19]. Nevertheless, the superficial boron concentration used in [19] was 1×10^{15} cm^{-3}, while the superficial boron concentrations in this work are from two to three orders of magnitude higher. Therefore, these surface base doping concentrations could change the dominant transport mechanism due to a higher probability of tunneling.

In Fig. 4(b) *Rs* is plotted as a function of the temperature, and an $(E_C - E_F)$ of 0.12 $\pm$ 0.015 eV was calculated. This value is consistent with the activation energy determined from the dark conductivity measurements of the amorphous layers, and with the value estimated from the gas flow ratio of $[PH_3]/[SiH_4+PH_3]$ [12].

B. Reverse dark J-V characteristics

In previous works [7-9], several authors found that the reverse current density (J_R) followed the relationship $J_R{}^2 \alpha V$. As shown in Fig. 5, $J_R{}^2$ is a fairly linear function of the reverse voltage from 0 to 0.5 V for W1 and W3. From this behavior, we can say that J_R is dominated by the carrier generation inside the space charge region. Also, Fig. 6 shows J_R as a function of temperature at V_R = -0.1, - 0.3 , - 0.5 and -0.7 V, resulting in $Eac_{reverse}$ = 0.72 and 0.68 eV. These values are close to $Eg_{n\text{-}type\ a\text{-}SiGe:H}/2$, showing that the electrical behavior is determined by the carrier generation in the *n*-type *a*-SiGe:H film. On the other hand, the heterojunctions fabricated on W2 and W4 do not follow this relationship. Thus, the carries generated in the depletion region do not dominate the reverse current. In W2, the J_R dependence on temperature is described as [17]:

$$J = A_H \exp\left[-\frac{B}{T^{\frac{1}{N}}}\right] \qquad (8)$$

where A_H is a weakly temperature dependent quantity, *B* is a constant, and *N* is a constant whose value can be 4 or 3. If *N* = 4, eq. (8) corresponds to the $T^{-1/4}$ Mott's law, which is applicable for the transport in the three dimensional case, whereas the two dimensional case corresponds to a $J \alpha T^{-1/3}$ behavior. For W2 we found that J_R is proportional to $T^{-1/3}$ at -0.5, -1.0 and -1.5 V, and the linear fits present approximately the same slopes (see Fig. 7). These results suggest that the reverse current is influenced by the thermally activated electron contribution from the deep traps. Finally, Figure (8) shows that the heterojunctions in W4 follow none of the previous reported transport mechanisms. In this case J_R can be due to thermionic field

Table 2. Basic charge transport mechanisms

Transport Mechanism	J_0	A	η
Diffusion	$J_0 \alpha \exp\left[\frac{Eg}{kT}\right]$	$A = \frac{q}{kT}$	$\eta = 1$
Recombination	$J_0 \alpha \exp\left[\frac{Eg}{2kT}\right]$	$A = \frac{q}{\eta kT}$	$\eta \leq 2$
MTCE	$J_0 \alpha \exp\left[\frac{Eac_{tun}}{kT}\right]$	$A = const$	$\eta \neq const$
Multistep tunneling	$J_0 \alpha \exp[\gamma T]$	$A = const$	$\eta \neq const$
Thermionic	$J_0 \alpha \exp\left[-\frac{\phi_B}{kT}\right] kT^{\frac{3}{2}}$	$A = \frac{q}{kT}$	$\eta = 1$

emission (TFE), which occurs in metal-semiconductor junctions or heavily doped junctions [15].

C. C-V characteristics

The *C-V* characteristics of the heterojunctions were measured at a frequency of 100 KHz using a Keithley 590 *C-V* analyzer precision meter. The capacitance per unit area of an anisotype heterojunction is described by the Anderson's model, which can be expressed as [20]:

$$C = \sqrt{\frac{qN_D N_A \varepsilon_a \varepsilon_c \varepsilon_0}{2[\varepsilon_a N_D + \varepsilon_c N_A][V_D - V]}} \qquad (9)$$

where q is the electronic charge, ε_0 is the permittivity of vacuum, ε_a and ε_c are the dielectric constants of the *n*-type *a*-SiGe:H film and *c*-Si, respectively; N_D and N_A are the doping concentrations of the *n*-type *a*-SiGe:H and the *p*-type crystalline-silicon, respectively; V_D is the diffusion voltage (the voltage drop trough the *n-p* junction in thermal equilibrium) and V is the applied voltage. Figure 9 shows the $1/C^2$ - V measured curves, where a linear behavior is observed in the 0.0 to -1V range. This fact is a clear indication that the fabricated diodes are abrupt junctions. From the same figure, V_D was obtained as 1.10, 1.15, 1.15, and 1.15 V for the wafers W1, W2, W3, and W4, respectively**.** The same $1/C^2$-V curves were used to evaluate the impurity concentration of the lightly doped side. Thus, from the slopes of the $1/C^2$ - V curves of W2 and W4, we estimated an average doping concentration around 2×10^{17} cm^{-3} for the *n*-type *a*-SiGe:H film, which agrees with the average free carrier concentration estimated in [12].

For the electrical characterization of any kind of heterojunctions, one of the main issues is the evaluation of the conduction and valence band discontinuities, ΔE_C and ΔE_V. A simple solution was proposed by Anderson [21] based on a previous work by Shockley [21]. This model has been used satisfactorily for the analysis of amorphous/*c*-Si and nanocrystalline/*c*-Si heterojunctions [20, 22]. The Anderson's equations state the following:

$$\Delta E_C = \chi_{Si} - \chi_{n-type\ a-SiGe:H} \qquad (10)$$

$$\Delta E_V = E_{g\ n-type\ a-SiGe:H} - E_{g\_Si} - \Delta E_C \qquad (11)$$

where $E_{g\ n\text{-}type\ a\text{-}SiGe:H}$ and $\chi_{n-type\ a-SiGe:H}$ are the optical band gap and the electron affinity of the n-type a-SiGe:H film, respectively; $E_{g\text{-}Si}$ and χ_{Si} are the band gap and electron affinity of the *p*-type *c*-Si. Using the data presented in [12], $E_{g\ n\text{-}type\ a\text{-}SiGe:H}$ = 1.4 eV and $\chi_{n-type\ a-SiGe:H}$ = 4.04 eV. From [23], we used $E_{g\text{-}Si}$ = 1.12 eV and χ_{Si} = 4.05 eV for p-type c-Si with doping concentrations of 7×10^{16} and 7×10^{17} cm^{-3}, respectively. For a higher doping concentration, $5x10^{18}cm^{-3}$, the bandgap narrowing effects were taken into account using the Jain and Roulston's equations [24]. Using these data in eqs. (10) and (11), the following results are obtained: ΔE_C = 30, 40, 40, and 40 meV and ΔE_V = 250, 240, 240, and 240 meV for the heterojunctions of W1, W2, W3, and W4, respectively. In any case the values of the conduction and valence band discontinuities should be considered as a first approximation.

It is worth mentioning that these *C-V* measurements confirmed that the valence band discontinuity is much higher than the conduction band discontinuity. This

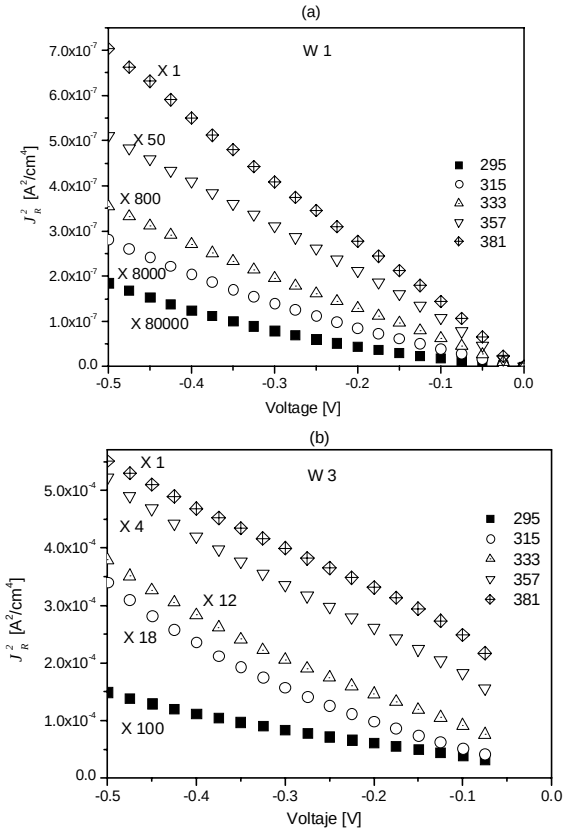

Figures 5. Amplified values of $J_R^{\ 2}$ for W1(a) and W3 (b), respectively, the factors are shown in the figures.

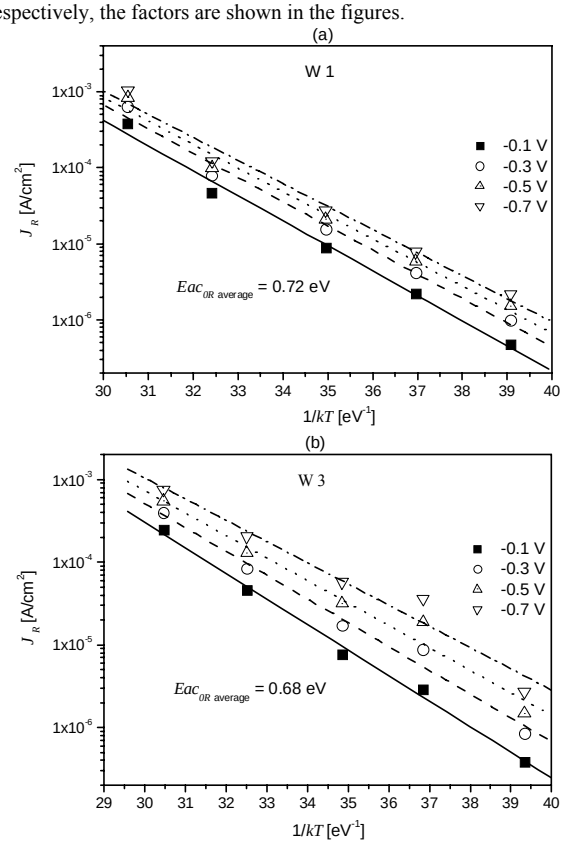

Figure 6. J_R measurement at Vr = 0.1, 0.3, 0.5 and 0.7 V as a function of the temperature for W1 (a) and W3 (b), respectively.

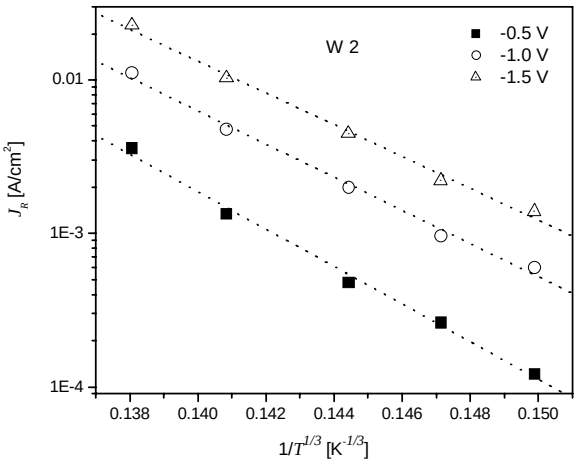

Figure 7. Temperature dependence of the current density at reverse bias of = -0.5, -1 and -1.5 V for W3.

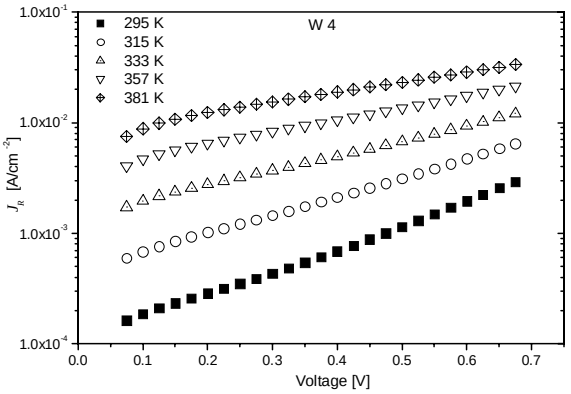

Figure 8. J_R versus reverse bias voltage as a function of temperature for W4.

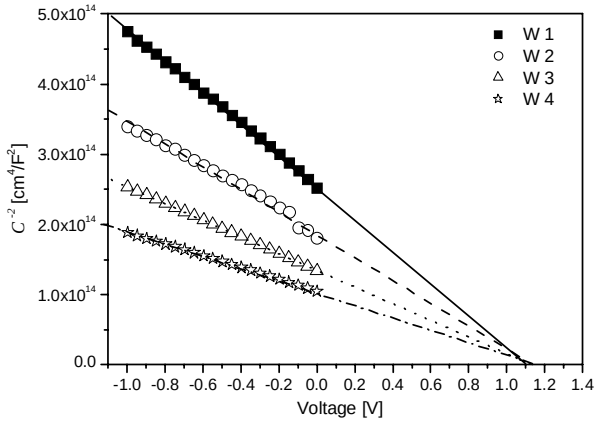

Figure 9. Reverse of the square capacitance versus applied voltage for all the n-type a-SiGe:H/ p-type c-silicon heterojunction diodes.

together with the fact that η is close to1, suggest that the heterojunctions fabricated in W1 and W3 can be used as a base-emitter diode for an amorphous/crystalline-silicon HBT. However, both parameters, the activation energy and η do not depend on the base doping concentration (Figs. 3 and 4). This electrical behavior is due to the broader band tails in these thin amorphous layers, which leads to some increase of the recombination current density in the amorphous film. Thus, if this heterojunction were used to fabricate HBT devices, the common-emitter gain current could be decreased considerably. To overcome this drawback, the density of states in the thin amorphous layer, or alternatively the base doping concentration must be reduced. Nevertheless, a low base doping concentration imposes a severe restriction for the HBT performance, since this could lead to a wider base region and then decreasing the cutoff frequency. On the other hand, the density of states in the noncrystalline films can be reduced by using a microcrystalline film instead of the thin amorphous layer, or by inserting a crystalline silicon region between the amorphous film and the base region [25].

4. Conclusions

In this work, we have analyzed the influence of the base doping concentration and emitter thickness on the current transport mechanisms for *n*-type *a*-SiGe:H on *p*-type *c*-Si heterojunctions. The capacitance-voltage measurements confirmed the existence of an abrupt junction, whereas the conduction and valence band discontinuities were estimated using the Anderson rule. This analysis shows that the valence band discontinuity is much higher than the conduction band discontinuity.

For the forward bias regime, the current-voltage measurements show that the transport mechanisms are strongly influenced by the emitter thickness. For thin emitters in the $0 < V < 0.45$ V bias range, the transport mechanism is dominated by carrier recombination in the *a*-SiGe:H depletion region, whereas multistep tunneling through the depletion region was the main transport mechanism for the heterojunctions with thicker emitters. This analysis leads to the conclusion that the base doping concentration does not play an important role on the transport mechanisms for the *n*-type *a*-SiGe:H/*p*-type *c*-Si heterojunctions. For a $V \geq 0.45$ V forward bias, the space charge limited effect becomes the main transport mechanism for all the devices.

For the thin emitter heterojunctions under reverse bias condition, the transport mechanism is dominated by carrier generation in the amorphous space charge region.

For the thick emitter heterojunction under reverse bias condition, hopping through localized states inside the amorphous bandgap is the main transport mechanism for the wafers with a base doping concentration of 7×10^{17} cm^{-3}, whereas a TFE transport mechanism is dominant for a base doping concentration of 5×10^{18} cm^{-3}.

Finally, thin *n*-type *a*-SiGe:H films as those used to fabricate our heterojunctions have been analyzed, and hence they are proposed as a key material to fabricate high-performance HBTs. Our measurements have shown that the density of states in the amorphous film must be reduced in order to minimize the space charge recombination current, because the reduction of the density of states could lead to HBTs with a higher current gain and higher cut off frequency.

Acknowledgements

We would like to acknowledge the technicians at the INAOE Microelectronics Laboratory: M. Landa-Vázquez, P. Alarcón-Peña, N. Carlos-Ramírez, A. Itzmoyotl-Toxqui and I. Juárez-Ramírez for their assistance during the fabrication and characterization of the devices.

Rererences

[1] A. I. Kosarev, A. J. Torres, C. Zuñiga, A. S. Abramov, P. Rosales, and A. Sibaja, *J. of Mat. Res.* **18**, 1918 (2003).
[2] R. Ambrosio, A. Torres, A. Kosarev, C. Zúñiga, and A. S. Abramov, *Latin American Circuits and Systems*, INAOE, Puebla Mexico. **1,** 18 (2002).
[3] W. Luft and Y. S. Tsuo, Hydrogenated amorphous silicon alloy Deposition processes 1ed. (Marcel Dekker, Inc., 1993).
[4] Rubí Salazar Amador, *Diseño, Fabricación y Prueba de un Detector de Barrera Shocttky de a-SiGe:H/p-Si para el Rango Medio del Infrarrojo,* Phd. Thesis INAOE, (Sta. María Tonantzintla, Puebla, México, 2002)
[5] M. L. García Cruz, A. Torres, A. Kosarev, R. Ambrosio, *Journal of Non-Crystalline Solids.* **329**, 179 (2003).
[6] A. Heredia-J, A. Torres-J, F.J. De la Hidalga-W, A. Jaramillo-N, J. Sánchez-M, C. Zúñiga-I., M. Basurto-P., and A. Pérez, *Mat. Res. Soc. Symp. Proc.* V2.4.1, **796** (2004)
[7] H. Matsuura, *IEEE-TED*. **36**, 2908 (1989).
[8] L. F. Marsal, J. Pallarés, X. Correig, A. Orpella, D. Bardés and R. Alcubilla, *J. Appl. Phys*. **85** , 1216 (1999)
[9] L. F. Marsal, J. Pallarés, X. Correig, J. Calderer, and R. Alcubilla, *J. Appl. Phys.* **70**, 8493 (1996).
[10] Ping Li, Yong Q., and C. Andre T. Salama, *IEEE-TED*, **41**, 932 (1994).
[11] Z. R. Tang T. Kamins, and C. Andre T. Salama, *IEEE-TED*, **14**, 348 (1993).
[12] P. Rosales-Quintero, A. Torres-Jacome, R. Murphy-Arteaga F. J. De la Hidalga Wade, L. F. Marsal, R. Cabré, and J. Pallarès *J. Appl. Phys*. **97** 083710 (2005).
[13] Werner Luft and Y. Simon Tsuo, *Hydrogenated Amorphous Silicon Alloy Deposition Process,* 1ed. (Marcel Dekker, Inc., 1993).
[14] H. Matsuura, and H. Okushi**,** *Amorphous and Microcrystalline Semiconductor Devices*, 1 ed. (edited by J. Kanicki Artech House, Boston, MA, Vol. 2, 1992)
[15] R. J. Nemanich, and M. J. Thompson *Metal Semiconductor Schottky Barrier Junctions and Their Applications*, 1ed. (edited by B. L. Sharma Plenum, New York, 1984).
[16] A. Rose, *Phys. Rev*. **97**, 1538 (1955).
[17] L. F. Marsal, J. Pallarés, X. Correig, J. Calderer, and R. Alcubilla, *Semiconductor Sci. and Technol*, **11**, 1209 (1996).
[18] A. J. Harris, R. S. Walker, and R. Sneddon .*J. Appl. Phys*. **51**, 4287 (1980).

[19] P. Rosales-Quintero, A. Torres-Jacome, R. Murphy-Arteaga and M. Landa-Vázquez, *Semiconductor Sci. and Technol*. **19**, 366 (2004).
[20] L. Magafas, N. Georgoulas and A. Thanailakis, *Semiconductor Sci. and Technol*. **7**, 1363 (1992).
[21] R. L. Anderson, *Solid-State Electron*. **5**, 34 (1962).
[22] X. Gangy and W. Tianmin, *Semiconductor Sci. and Technol.* **15**, 613 (2000).
[23] Sze S. M. Physics of Semiconductor Devices, 2 ed. (Wiley, 1981)
[24] S. C. Jain and D. J. Roulston, *Solid-State Electron*, **34**, 453 (1991).
[25] D. M. Garner and G. A. J. Amaratunga, *Solid State Electronics*, **43**, 1973 (1999).